Spray-Pyrolyzed ZnO as Electron Selective Contact for Long Term Stable Planar $CH_3NH_3PbI_3$ Perovskite Solar Cells.

Thi Tuyen Ngo[1], Eva M. Barea[1], Ramon Tena-Zaera[2] and Iván Mora-Seró[1,*]

[1] Institute of Advanced Materials (INAM), University Jaume I, Avenida de Vicent Sos Baynat, s/n, 12006 Castelló de la Plana, Castellón (Spain)
[2]CIDETEC, Parque Tecnológico de San Sebastián, Paseo Miramón, 196, Donostia–San Sebastián 20014 (Spain)
[*] Corresponding author: sero@uji.es

Key words: ZnO, electron selective contacts, perovskite, solar cells, long term stability.

Abstract

Electron selective contacts (ESCs) play an important role in the performance of perovskite solar cells (PSCs). ZnO has attracted an important attention as a good material for ESCs because of its matched energy levels with those of perovskite, its high transmittance in the visible region and its high electron mobility. Here we reported the use ZnO thin layers prepared by spray pyrolysis as ESC for PSCs. Our ZnO based planar $CH_3NH_3PbI_3$ ($MAPbI_3$) devices were not only stable in a humidity of 35% but also improved the performance even after more than 1 month of preparation, due to an increase of charge transfer at the ZnO interface as it has been characterized by Impedance Spectroscopy. The formation of ZnO depending on the preparation conditions such as gas flow, zinc acetate solution concentrations and substrate temperatures effect on the performance of stability of $MAPbI_3$ solar cells, and also the low-hysteresis reported for these samples were discussed in this study. We have also observed that long term structural evolution of perovskite film also depends on the ZnO substrate and its deposition method.

1. INTRODUCTION.

Perovskite solar cells (PSCs) have developed rapidly over the past few years due to the promising properties of perovskite materials such as high absorption over the visible range and long diffusion length. The power conversion efficiency of PSCs has been recorded over 22%.[1] Such high performance of PSCs needs not just an outstanding perovskite absorber layer but also excellent selective contacts for an optimum charge separation. As a result, the design and materials properties of the selective contacts are crucial for solar cell performance.[2-6] Concretely, the electron selective contact (ESC) is a blocking layer that prevents holes from reaching the transparent conductive electrode, fluorine-doped tin oxide (FTO), avoiding interfacial recombination. For high performance solar cells, ESCs should meet the following criteria: (a) good optical transmittance in the visible range, which reduces the optical energy loss; (b) the energy levels of ESCs should match that of perovskite materials, which improve the electron extraction efficiency and block holes; (c) good electron mobility; (d) high film quality by easy fabrication methods.[6]

Among the ESC materials, ZnO has attracted much attention to be used as an ESC in DSSCs and polymer solar cells,[7] but also in PSCs since the early stages.[8] Because, first of all, ZnO has a very high transmittance in the visible spectra and more importantly ZnO has a proper bandgap, energy band alignment suitable with those of perovskite. Second, ZnO possesses a very high electron mobility (bulk ZnO 205-300 cm^2V^{-1} s^{-1} and nanowire ZnO 1000 cm^2V^{-1} s^{-1}) which can potentially improve the electron transport efficiency and reduce the recombination loss.[3, 9, 10] Third, the extraction properties of ZnO may be maintained if no chemical reaction between ZnO and CH_3NH_3I is produced,[11] although for certain ZnO surfaces (i.e. including some absorbates) deprotonation of $CH_3NH_3^+$ (MA) cation may occur during thermal treatments.[3] Fourth, various ZnO nanostructures such like nanowires,[12] nanotubes,[13] nanobelts,[14] nanorings,[15] nanoflowers,[16] nanorods,[17] and so on, can be easily fabricated by controlling the growth rates along different directions.

Recently ZnO as ESC for PSCs has been studied systematically.[3, 8, 18-22] In 2015 Jiaxing Song's group published a PSCs glass/ITO/ZnO/$MAPbI_3$/spiroOMeTAD/Ag structure given a conversion efficiency of 13.9%. Interestingly their devices exhibited a good stability, with a conversion efficiency that was maintained around 90% after 22 days exposed to ambient condition.[23] In the same year, Qin Hu et al. modified ZnO layer by linking it with polymer and increased the conversion efficiency to 15.96%.[24] By using triple cation perovskite absorber 2 years later Jiaxing Song et al. reported 18.9% of conversion efficiency ZnO based PSCs,[25] confirming the possibility to use ZnO as efficient ESCs in PSCs.

In this study, we used a spray pyrolysis method, which is low cost and quite suitable for large area thin films with good reproducibility, to prepare ZnO thin layers. Using spray-pyrolyzed ZnO thin films, we prepared planar PSCs following a structure FTO/ZnO/$MAPbI_3$/Spiro OMeTAD/Au and focused on their stability. In which ZnO thin films were spray-pyrolyzed with different conditions such as different gas flow (N_2 or O_2), substrate temperatures and zinc acetate solution concentrations. Our devices not only presented a very good stability but also the performance improvement even after 34 days storing at around 35% of humidity.

2. EXPERIMENTAL SECTION

2.1. Device preparation

ZnO thin layer. Substrates (SnO_2:F, FTO or SnO_2:In, ITO) substrates were sonicated in distilled water with soap, distilled water, ethanol and propanol-2 for15 minutes and then treated with an UV−O_3 lamp for 15 minutes. The ZnO layer was deposited by spray pyrolysis with 2 different recipes. For the first recipe, the synthesis of ZnO was performed according to procedure previously reported with some modification.[26] Briefly, ZnO was spray pyrolyzed from 5 ml solution containing 0.3M zinc acetate dihydate in a mixed of distilled water and propanol-2 (1:1 volume ratio). The pH of zinc acetate solution was adjusted to 4 by adding acetic acid. When FTO substrate temperature reached to 450°C, zinc acetate solution was sprayed on their surface using N_2 or O_2 flow. After spraying, ZnO layer was annealed at the same temperature (450°C) for 30 minutes then cooled to room temperature.

For the second recipe, the concentration of zinc acetate solution was reduced to 0.1M. And distilled water was mixed with ethanol instead of propanol-2 with a volume ratio 1:3. Acetic acid was also added to the solution to produce a pH of 5. ZnO layers were deposited on FTO and ITO at different substrate temperatures from 300°C to 450°C (300°C for ITO) and from different zinc acetate volumes. After spraying, ZnO was also annealed for 30 minutes. O_2 flow is used in these cases.

To simplify, ZnO films obtained from N_2 and O_2 flow were named ZnO_N_2 and ZnO_O_2 respectively.

Perovskite. Perovskite solution was prepared by dissolving 622 mg (1.35 mmol) of PbI_2 and 215 mg (1.35 mmol) of MAI in a co-solvent containing 1ml of N,N-dimethylformamide (DMF) and 95 µl of dimethyl sulfoxide (DMSO). A thin film deposition was done inside a glove box by spin coating 50 µl of perovskite solution at 5000 rpm. Diethyl ether was added to the film when the spin coater was running, 5-6s after the spinning starts. Finally perovskite film was annealed at 100°C for 3 minutes.

Spiro OMeTAD and Gold. Spiro OMeTAD solution was prepared by dissolving 72.3 mg of spiro-OMeTAD (2,2′,7,7′-tetrakis(N,N-di-p-methoxyphenylamine)-9,9-spirobifluorene) was dissolved in 1 ml of chlorobenzene, then mixed with 28.8 µl of 4-tertbutylpyridine and 17.5 µl of a stock Li^+ solution (which contained 520 mg/ml bistrifluoromethylsulfonylamine lithium salt in acetonitrile). Spiro OMeTAD layer was

spin coated on perovskite films at 4000 rpm for 30s. Finally, 60 nm of gold were thermally evaporated in an ultrahigh vacuum chamber on top of Spiro OMeTAD layer to make complete devices.

2.2. Film and device characterization

Thin film characterization. The morphology and structural properties of the ZnO and $MAPbI_3$ perovskite films was analysed by scanning electron microscopy (SEM) using a JSM7001F (Field emission scanning electron microscope), a Bruker AXS-D4 Endeaver Advance X-ray(XRD) using Cu Kα radiation respectively. Absorbance of those films were measured by using a Cary 300 Bio UV-VIS spectrophotometer. And photoluminescence (PL) spectra of $MAPbI_3$ films were obtained by using a spectrophotometer based on a CCD detector (Andor-iDUSDV420A-OE) coupled with a spectrograph as a diffraction grating (Newport 77400). A commercial continuous laser diode (650 nm, 5 mW) was used as an excitation source. Morphology and conductivity of ZnO films were investigated using Atomic Force Microscopy. The morphology of the ZnO films was investigated using AFM (Concept Scientific Instrument) in resiscope mode. While the current maps of the ZnO films were recorded using a diamond coated tip at an applied bias of 1V in N_2 flow.

Device characterization. J–V curves of solar cells were measured under a xenon arc lamp simulator equipped with an AM 1.5 spectral filter (Sun 2000, ABET Technologies). The intensity was adjusted to provide 1 sun (100 mW cm^{-2}) by using a calibrated silicon solar cell. The J–V characteristics were recorded by scanning the potential from high voltage to zero (backward scan mode, BW) and from zero to high voltage (forward scan mode, FW) at ≈45 mV/s. The IPCE measurements were performed employing a 150 W xenon lamp coupled with a computer-controlled monochromator; the photocurrent was measured using an optical power meter 70310 from Oriel Instruments, using a Si photodiode to calibrate the system. Electroluminescence (EL) experiments were performed by applying an electric field in the perovskite layer integrated in a diode configuration and collecting the emission of the film with a similar set-up of PL measurement. Measurements have been carried out using a non-sealed sample holder. Sample holder has a gas connection to flow N_2 continuously during the EL measurements. The EQE estimations were performed by calibrating the optical equipment with a commercial GaAs infrared LED (model EL-23G, peak emission centered at λmax = 940 nm, 28.3 W sr^{-1} m^{-2}).

3. RESULTS AND DISCUSSION

ZnO thin films were deposited by spray pyrolysis method. It is worth to mention that spray pyrolysis itself is a method which involves spraying a solution onto a heated substrate. The droplets of a spray solution, after hitting on the substrate surface, spread into a disk shaped structure and undergo thermal decomposition. The shape and size of the disk depends on the momentum and volume of the droplet. Consequently, the film will be initially composed of overlapping disks which will finally become grains with specific orientation on the annealed substrate.[26] It has been previously discussed that many factors can affect on the film formation such as spray rate, precursor solution[26] (nature of solvents, type of salts and

concentration), substrate temperatures[27] and so on. All these factors influence the morphology and the structural, electrical and optical properties of spray-pyrolyzed films.[26, 27] In agreement with previous discussions, we also found that the morphology dependence of ZnO films formed at different substrate temperatures (see Figure S1).

In this study, the ZnO films were deposited with different gas components, N_2 and O_2 flows. Figure 1a shows the absorbance, transmittance spectra and top view SEM of ZnO films deposited on FTO which obtained by spraying zinc acetate using two these different gas, during the spray pyrolysis process. In agreement with literature, our ZnO films are very transparent in the visible range.[28] This fact contributes to reduce the optical losses. The ZnO films obtained from N_2 and O_2 flow have a similar morphology, see Figure 1b and 1c. However, ZnO_N_2 exhibits slightly bigger grains. And this difference in grain size is also confirmed by AFM measurement (see Figure S2). ZnO deposition process is carried out in ambient condition. Consequently, even we used N_2 flow, O_2 from air is presented during ZnO film formation. Consequently, the main difference between the ZnO depositions is the different ratio of O_2 in the gas, being obviously much higher when O_2 flow is used. Tseng et al. reported the ZnO deposition by sputtering from a mixed Ar and O_2 gas with different ratio of O_2.[28] In their study, they observed no influence of gas on ZnO crystallinity and morphology. However, it is important to note that all their ZnO films were obtained without substrate heating while our spray-pyrolyzed ZnO was archived with substrates heated at 450^{o}C. The differences in substrate heating temperatures and O_2 ratio in the gas may explain the grain size difference of ZnO obtained with N_2 and O_2 flow respect previous reports in the literature.

In addition to the grain size dependence, we also observed the optical band offset dependence on the components of gas used during the ZnO spray pyrolysis process. As seen in the Figure 1a and S3a, ZnO spray-pyrolyzed with O_2 flow shows slightly larger bandgap than ZnO prepared with N_2 flow. This fact is in agreement with previous literature in which it has been reported that the bandgap of spray-pyrolyzed ZnO can be modified by changing the spray conditions such as spray rates, spray solution concentrations and substrate temperatures.[26, 27] In the range of temperatures employed (~350^{o}C) the amount of oxygen in the gas used affects on the decomposition and oxidation of precursors in the solution, resulting in different properties, including the optical properties, of the ZnO thin films. Additionally, we also found that the concentration of a spray solution can change the bandgap of spray-pyrolyzed ZnO as well (see Figure S3b). However, the volume of a spray solution does not change the absorption offset of ZnO films. Increasing the volume

only results on the deposition of a thicker films with the consequent increase of absorption (See Figure S3c).

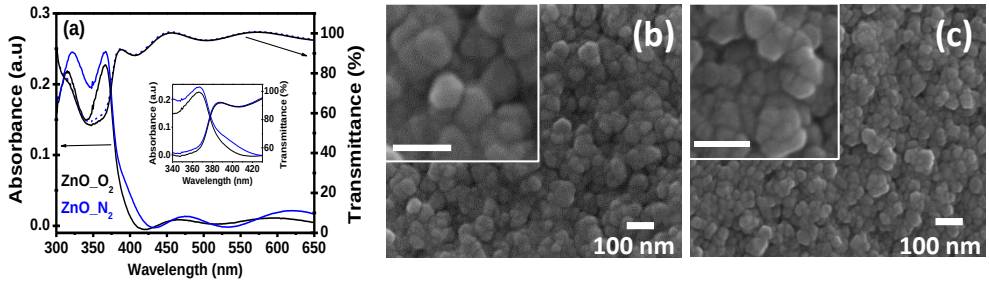

Figure 1. (a) Absorbance and transmittance; and SEM images from secondary electrons of ZnO layer deposited on FTO from 0.3 M zinc acetate solution at 450°C with (b) nitrogen (named ZnO_N_2) and (c) oxygen flow (named ZnO_O_2), bar scale in insect is 100 nm.

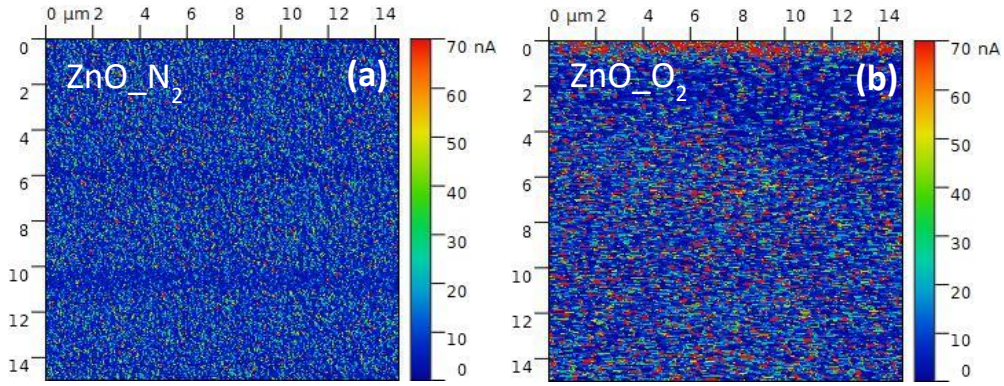

Figure 2. Conductive atomic force microscopy (C-AFM) of ZnO layer deposited on FTO from 0.3 M zinc acetate solution at 450°C with nitrogen (a, named ZnO_N_2) and oxygen flow (b, named ZnO_O_2).

We moreover archived the difference in the conductivity of spray-pyrolyzed ZnO films obtaining by using N_2 or O_2 flow. The conductive atomic force microscopy measurement pointed out both those ZnO films contain homogeneous current contribution on the surface. However ZnO_N_2 exhibits lower current, indicating lower conductivity than ZnO_O_2 (see Figure 2), as impedance spectroscopy analysis also confirms, see below. It has been previously reported that the concentration and pH of a spray solution, and spay rate can affect on the electrical resistivity of ZnO films.[26] Here we found that the components of gas used in a spray pyrolysis also play a role in a conductivity of formed films.

The absorbance spectra of fresh $MAPbI_3$ films deposited on ZnO prepared with N_2 and O_2 flow show a strong absorption at the wavelength between 400 nm to 800 nm (see Figure S4a). No difference between the absorbance spectra of $MAPbI_3$ films coated on ZnO_N_2 or ZnO_O_2 thin layers were observed, indicating no thickness difference. Figure S4b and S4c present the cross section of fresh $MAPbI_3/ZnO\_N_2$ film. Both ZnO compact and $MAPbI_3$ perovskite layers are very homogeneous and fully coverage, with 50 nm and 270 nm thickness, respectively. The photoluminescence (PL) spectra of those perovskite layers deposited on ZnO_N_2 or ZnO_O_2 substrates were similar as well (see Figure S4a). $MAPbI_3$ perovskite coated on ZnO_N_2 and ZnO_O_2 presents the tetragonal structural phase, with (110) preferential orientation, with diffraction peak at 14.2^o, see Figure S5a and S5b. However, the degree of preferential orientation is not exactly the same for both fresh samples as fresh $MAPbI_3/ZnO\_O_2$ presents higher X-Ray Diffraction (XRD) intensity at peak 14.2^o diffraction compared with fresh $MAPbI_3/ZnO\_N_2$, see Figure S5c. This finding is in agreement with the observation of Tseng's group.[28] Smaller full width at half maximum (FWHM) of fresh $MAPbI_3$ coated on ZnO_O_2 (see Figure S6a and Table S1) suggests higher perovskite crystallite size is obtained.

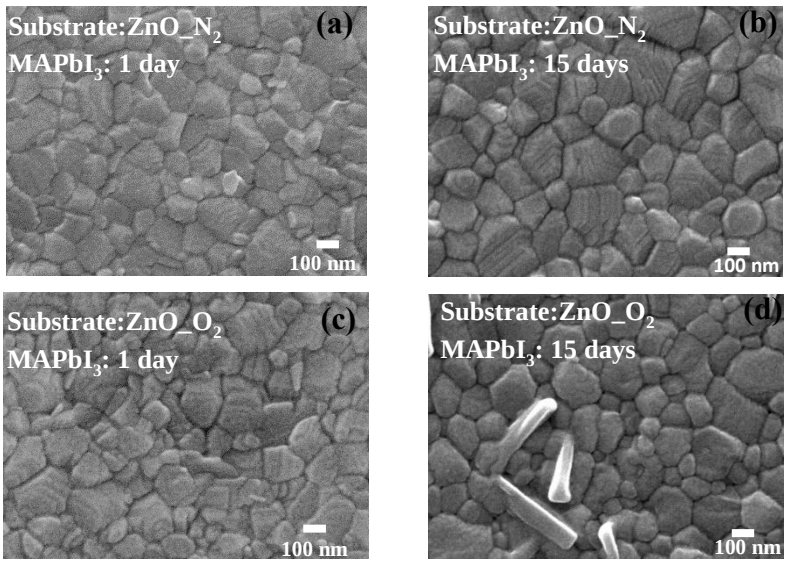

Figure 3. (a-d) Top view of 1 day and 15 days-old $MAPbI_3$ deposited on FTO/ZnO_N_2 (a-b) and FTO/ZnO_O_2 substrates (c-d). $MAPbI_3$ films were stored under dark and at room temperature and at around 35% of humidity.

Figure 3 presents Scanning Electron Microscopy (SEM) images of the top view of fresh and old $MAPbI_3$ films deposited on ZnO prepared with both N_2 and O_2 flows. The top view SEM of fresh $MAPbI_3/ZnO\_O_2$ also shows slightly bigger grain size than fresh $MAPbI_3/ZnO\_N_2$, see Figures 3a and 3c. This observation is

in agreement with XRD measurement, higher XRD intensity and lower FWHM at peak 14.2° fresh for $MAPbI_3/ZnO\_O_2$ film (Figure S5c, S6a and Table S1). It is worth to note that in XRD measurement, we did not observe the XRD pattern of ZnO due to its extremely thin thickness (see Figure S5a and b). Thus we could not analyse the dependence of ZnO structure on the components of gas used.

However, the most interesting feature regarding the samples morphology is observed after aging. The morphology of $MAPbI_3$ films deposited on ZnO_N_2 and ZnO_O_2 changed oppositely after 15 days stored at room temperature under dark and at around 35% of humidity conditions. For ZnO_N_2 substrate, $MAPbI_3$ film showed an increase in grain size for a 15 days-old film, see Figure 3a and 3b. Evolution of FWHM in XRD (i.e. crystallite sizes) also points in the same direction, see Figure S5d, S6c and Table S1. Similar results obtained by the study of Roose et al. They prepared mixed halide cation perovskite (from a solution containing FAI, PbI_2, MABr, $PbBr_2$ and CsI) on SnO_2 compact layer. They demonstrated that smaller crystallites within perovskite films spontaneously coalescence into larger ones, even when complete devices are stored in the dark at room temperature.[29] It is important to note that our $MAPbI_3$ perovskite films are composed by pure iodine phase, which is known less stable than perovskite containing Cs cation, and stored at around 35% of humidity condition. Moreover the preferential orientation of $MAPbI_3$ film belong the plane (110) which is perpendicular to the substrate[30] is slightly improved after 15 days, see Table S1.

Oppositely to $MAPbI_3$ perovskite films deposited on ZnO_N_2 thin layer, aging perovskite coated on ZnO_O_2 substrate shows no appreciable change on grain size, see Fig 3c and 3d. A detailed analysis of XRD, see Figure S5e, S6b and Table S1, points to a decrease in the degree of preferential orientation along the (110) plane direction comparing aged cell with the fresh one, and also a slight increase of FWHM confirming the crystallite size evolution ZnO_O_2 is not similar to the observed for ZnO_N_2. Here we found that ZnO preparation method play an important role in the long term stability of $MAPbI_3$ perovskite. We have previously observed that kind of substrate, comparing organic PEDOT and several inorganic oxides had an impact on the perovskite degradation process.[31-34] Here we show that not just the substrate type but the preparation and termination method has influence on long term PSC stability.

It has been reported that the combination of light and O_2, in dry air, induced the degradation of $MAPbI_3$ perovskite films, and consequently the performance of solar cells. O_2 diffusion on $MAPbI_3$ films is accompanied by the photo-induced formation of highly reactive superoxide O_2^- species. This reactive O_2^- species can deprotonate the methylammonium cation (MAI^+) of photo-excited $MAPbI_3^*$,

leading to the formation of PbI_2, water, methylamine and iodine.[35-38] We have detected the formation of platelet-like grains, suggesting PbI_2, on $MAPbI_3/ZnO\_O_2$ film after 15 days, see Figure 3d and Figure S7b. However, note that in our storage conditions O_2 and water are presented but no illumination. Thus the required conditions for a degradation caused by a combination of light and O_2 were not fulfilled. On the other hand, it is well known that the presence of moisture can accelerate the degradation of $MAPbI_3$ perovskite. It is important to note that we stored $MAPbI_3/ZnO\_O_2$ and $MAPbI_3/ZnO\_N_2$ in the same conditions. And the platelet-like grains were clearly observed for aged $MAPbI_3/ZnO\_O_2$ samples while they were not clearly visible for aged $MAPbI_3/ZnO\_N_2$ films. The study of Nathan et al. pointed out that water adsorption of perovskite is heavily influence by the orientation of the methylammonium cations close to surface. And depending on methylammonium orientation, the water molecules can infiltrate into hollow site of the surface and get trapped.[39] As it has been discussed above, our ZnO spray-pyrolyzed with N_2 or O_2 flow gave different surficial termination which affected on the growth and orientation of perovskite coated on, and further affected on the water adsorption of perovskite. Thus, the presence of platelet-like grains ascribed to a water adsorption of perovskite could be related with the O_2 rich condition of ZnO formed in the spray pyrolysis process.

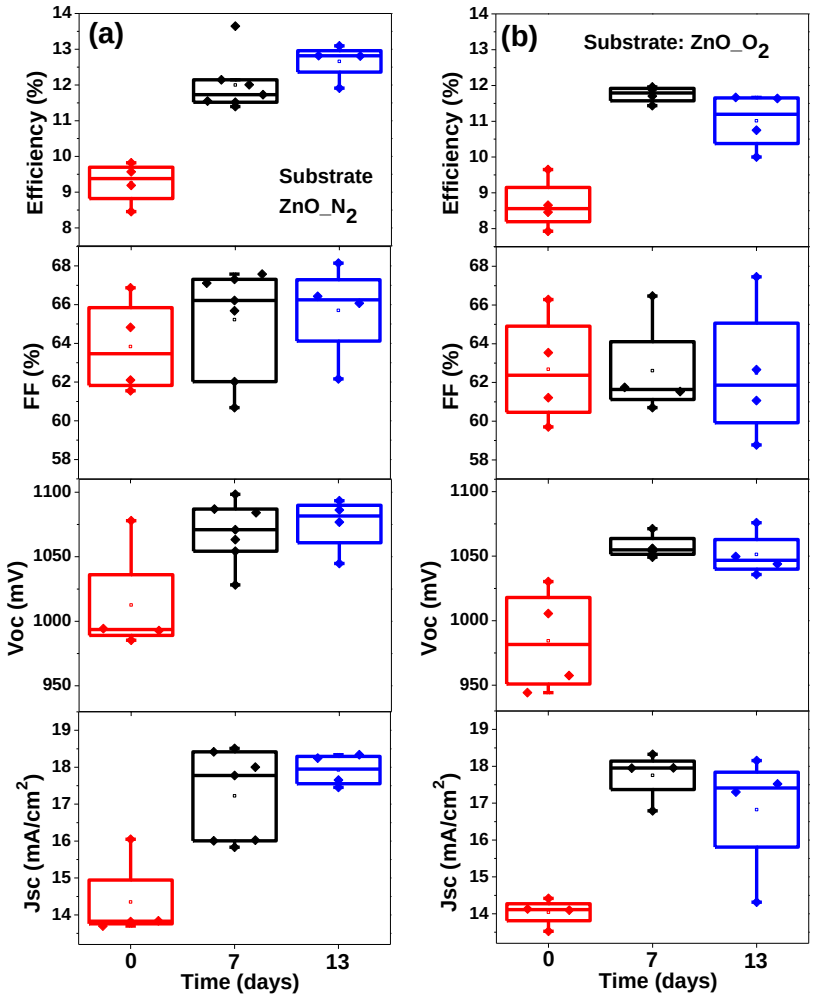

Figure 4. Performance at 1 sun illumination of planar based ZnO devices with a structure of FTO/ZnO/$MAPbI_3$/Spiro OMeTAD/Au respect to the time. In which ZnO was spray-pyrolyzed from 0.3 M zinc acetate solution at 450^{o}C with nitrogen (a) and oxygen flow (b). Full devices were stored under dark and at room temperature and at around 35% of humidity.

Table 1. Statistic photovoltaic parameters at 1 sun of planar based spray-pyrolyzed ZnO devices showed in the Fig 4.

Time (days)	**Substrate: ZnO_N_2**			
	Jsc [mA/cm^2]	Voc [mV]	FF [%]	Eta [%]
0	14.3 ± 0.2	1010.7 ± 8.3	61.3 ± 1	8.9± 0.1
7	17.5 ± 0.4	1066.5 ± 8.1	65.1 ± 1	12.1 ± 0.3
13	17.9 ± 0.2	1075.3 ± 10.8	65.7 ± 1.2	12.7 ± 0.3
Time (days)	**Substrate: ZnO_O_2**			
	Jsc [mA/cm^2]	Voc [mV]	FF [%]	Eta [%]
0	14 ± 0.2	984.4 ± 20.2	62.7 ± 1.4	8.7 ± 0.4
7	17.8 ± 0.3	1057.6 ± 4.8	62.6 ± 1.3	11.8 ± 0.1
13	16.8 ± 0.2	1051.4 ± 8.3	62.5 ± 1	11 ± 0.1

Full PSCs have been prepared using both kinds of spray-pyrolyzed ZnO layers with N_2 and O_2 flows, with a configuration of FTO/ZnO/$MAPbI_3$/spiro OMeTAD/Au. ZnO based PSCs were characterized by measuring the current density-voltage (J-V) curves under 1 sun illumination. Figure 4 presents the statistics of photovoltaic parameters of those devices respect to the fabrication time. Comparing the performance of PSCs fabricated using both ZnO substrates, no significant differences can be appreciated on fresh samples where ZnO_N_2 based devices showed slightly better performance on average, see Figure 4 and Table 1. However, fresh perovskite coated ZnO_O_2 shows slightly bigger grain sizes (Figure 3a and c), higher crystallinity and better preferential orientation along (110) planes (Figure S5c, S6a and table S1) than film coated ZnO_N_2 substrates. It has been previously reported that (110) planes of perovskite crystallites tends to align in the direction perpendicular with substrate and this preferential orientation influences the charge transfer and photovoltaic performance.[30] Thus, the lower performance obtained with ZnO_O_2 based devices could be due to different ZnO bandgap obtaining by using different gas, N_2 or O_2 flow (Figure 1a and S3a) and probable different band offsets. In the study of Tseng et al, they supposed for ZnO sputtered with Ar, the energy levels of conduction and valence bands down shift, which can enhance electron injection from perovskite to ZnO and block the hole more efficiently. They obtained better performance for devices containing ZnO sputtered with Ar,[28] the same trend as we observed with N_2.

Nevertheless the main difference on the performance of ZnO based PSCs depending on the deposition conditions is observed for aged samples. For ZnO_N_2 based PSCs, big improvements of 36% and 43% in photoconversion efficiency is observed after 7 and 13 days, respectively, see Figure 4a and Table 1. This improvement in average is due to the increasing of all solar cell parameters, photocurrent, J_{sc}, open circuit voltage, V_{oc} and fill factor, FF, but especially J_{sc}, see Figure 4 for the averaged results and Figure 5a for a single cell. This improvement

could be understood by the morphological and structural evolution experienced by these samples, as it has been previously discussed, with an increase in grain sizes, crystallinity and also in the degree of preferential orientation belong (110) plan of $MAPbI_3$ film deposited on ZnO_N_2, which is caused by the coalescence of smaller crystallites into larger ones.[29] Interestingly our ZnO_N_2 based devices presented the performance improvement not only until 13 days-age but also after more than 1 month, see Figure 5b. In addition, the measurement of incident photon to current efficiency (IPCE), Figure S8a, pointed out to a good agreement between the integrated photocurrent calculated from IPCE data and the J_{sc} measured from J-V curves, reverse scan, see Figure S8. In fact, these devices present low hysteresis as it can be appreciated for the champion cell an efficiency close to 14%, see Figure S9, in good agreement with the observation for other ZnO-based PSCs.[23, 24]

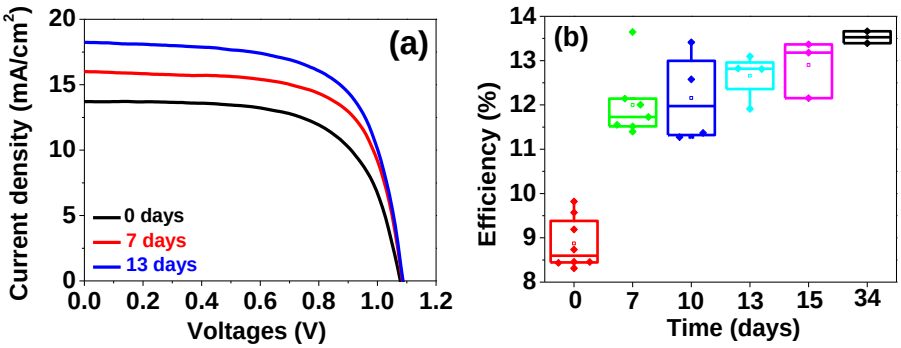

Figure 5. Current density-voltage (J-V) characteristic, reverse scan, (a) and efficiency (b) of FTO/ZnO_N_2/$MAPbI_3$/Spiro OMeTAD/Au at 1 sun illumination measured in different time. All devices were stored under dark at room temperature and at around 35% of humidity. ZnO was spray-pyrolyzed from 0.3 M zinc acetate solution at 450°C with nitrogen flow.

For ZnO_O_2 based PSCs, similar to ZnO_N_2 based devices, an enhancement of 36% in efficiency was observed after 7 days, see Figure 4b and Table 1. Then the performance of devices were slightly reduced after 13 days. The increase in conversion efficiency of ZnO_O_2 PSCs after 7 days should have the same origin with in ZnO_N_2 PSCs. The coalescence of smaller crystallite into larger ones also takes place in $MAPbI_3$ perovskite coated on ZnO_O_2. However, as discussed above, $MAPbI_3$/ZnO_O_2 films were degraded after 15 days of preparation, the crystallinity and preferential orientation along (110) plane were reduced, which causes a decrease in device performance. Note that $MAPbI_3$ films and devices were stored under the same conditions, see experimental section for more details. Thus the reduction in the performance after 13 days should be the results of the competition processes in $MAPbI_3$ films, which are (1) the coalescence of smaller crystallite into

larger ones and (2) the degradation caused by the interfacial defects induced by the O_2 rich fabrication conditions of the ZnO layers.

Interestingly the performance improvement after 7 days of preparation for ZnO_O_2 based PSCs was also obtained for spray-pyrolyzed ZnO at different FTO substrate temperatures, Figure S10 and Table S2. Additionally, we see again clearly that the ZnO spray pyrolysis conditions, in this case the substrate annealing temperatures, influences the performance of devices. The highest efficiency was obtained for fresh devices based on ZnO deposited at 350^{o}C. After 7 days, almost all the devices showed an improvement in efficiency. However, the efficiency enhancement was not the same for devices containing ZnO prepared at different temperatures. Moreover, as it can be seen in the Figure S1, ZnO fabricated at 350^{o}C (ZnO_350^{o}C) exhibits bigger grains than that deposited at 300^{o}C (ZnO_300^{o}C). And fresh PSCs based on ZnO_350^{o}C show higher efficiency than fresh PSCs based on ZnO_300^{o}C (see Table S2). The same trend is observed for devices containing ZnO_O_2 and ZnO_N_2 produced at 450^{o}C, where higher grain sizes (see Figure 1b and c) and higher performance were obtained for ZnO_N_2 based fresh PSCs (see Table 1). In addition, the concentration of ZnO spray solution also affects the performance of devices. Comparing ZnO_O_2 PSC devices prepared at 450^{o}C but with 2 different concentrations, 0.1M and 0.3M (named ZnO_0.1M and ZnO_0.3M respectively), ZnO_0.3M based PSCs gave a better performance (see Table 1 and S2). Note that the amount of Zn^{2+} in solutions was maintained the same. This behaviour can be attributed to the lower absorbance of ZnO_0.3M films which produced less optical loss (see Figure S3b).

Furthermore, the stability of ZnO_O_2 based PSCs also depends on the formation of ZnO. As showed above, the performance was slightly reduced after 13 days for devices containing ZnO_O_2 prepared from 0.3M zinc acetate solution and at 450^{o}C. However, ZnO_O_2 substrates prepared at lower zinc acetate solution concentration (0.1M) and lower substrate temperature (at 350^{o}C), exhibit an improvement of the performance even 30 days after their preparation, see Figure S11 and table S3.This analysis highlights that the use of O_2 flow is not the only parameter affecting the ZnO surface and consequently the PSC performance. The formation of ZnO depends on many factors, i.e. solution concentration, pH, temperature, gas and the flow rate, that needs an accurate optimization in order to get an appropriated ZnO surface termination not just for the fresh devices but for the aged ones with enhanced performance. The potential application of our ZnO deposition method has been verified for different substrates as FTO and ITO; and also different electronic devices as solar cells and LEDs as well, see Figure S12 and Table S4. And it is worth to note that our ZnO based PSC also presents a good performance recovered after the electrical injection (see Figure S13).

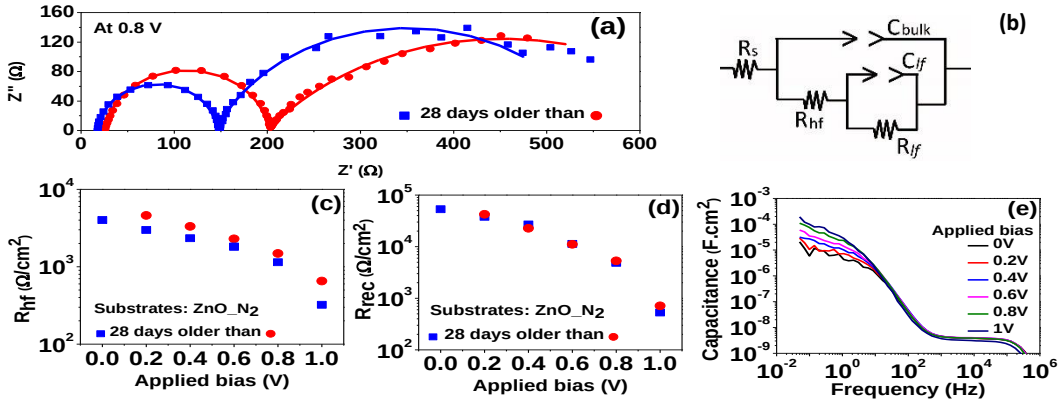

Figure 6. (a) Nyquist plot of perovskite devices based on ZnO_N_2 substrates, prepared on different time under 1 sun illumination at 0.8V DC applied bias, close to maximum power point voltage. Symbols correspond to the experimental points while solid line is the fitting of the impedance spectra using equivalent circuit in (b),[40-42] constant phase elements (PE) has been used instead of perfect capacitors for a better fitting. (c) R_{hf} related to charge transport and to the recombination and (d) the sum of R_{lf} and R_{hf} (R_{rec}) resistance related to the recombination of those devices respectively. (e) Capacitance at different applied bias of an older device presented in fig a-d.

For further understanding of the device behaviour, impedance spectroscopy measurements under working conditions, i.e. 1 sun illumination, at different applied DC voltages have been carried out. By comparing fitted data obtained from the impedance measurement of ZnO_O_2 and ZnO_N_2 based PSCs, we found that ZnO_O_2 based devices have lower contact series resistance, R_s (see Figure S14), indicating ZnO_O_2 is higher conductive than ZnO_N_2. This finding is in good agreement with the conductive AFM measurement (see Figure 2). However, the PSCs based on ZnO_N_2 or ZnO_O_2 have similar short circuit current (J_{sc}), (see Figure 4 and table 1).

We moreover measured the impedance spectroscopy of a fresh sample prepared on ZnO_N_2 substrates and of a sample prepared on the same substrate 28 days after its fabrication (see Figure 6a), under working conditions, i.e. 1 sun illumination, at different applied DC voltages. Nyquist plot presents two arc features at high frequency voltage (*hf*), left arc, and at low frequency (*lf*), right arc in Figure 6a. This is common feature observed in the impedance analysis of different kinds of PSCs, two regions at *hf* (higher than ~500 Hz) and *lf* (lower than ~500 Hz) can be differentiated.[43-45] However, in some cases arcs at *lf* or *hf* regions decouple in more than one arcs.[40, 43, 46] The experimental data obtained from impedance measurements have been fitted using the equivalent circuit depicted in Figure 6b.[40,

[41] Despites there is no full interpretation of the complete physical meaning of each one of these elements, the implications of some of them is qualitatively understood. It has been shown that $R_{rec}=R_{hf}+R_{lf}$ obtained from impedance spectroscopy analysis allows to reconstruct the J-V which implies that this resistance has a recombination character inversely proportional to the recombination rate.[41, 42] Figure 6d compares R_{rec} from fresh and aged sample and no significant difference can be appreciated. However, R_{hf} is clearly lower for aged sample (Figure 6c). It has been reported that this resistance receives contributions from the selective contacts and its decrease has been related with an increase of the charge transfer at the contacts with a consequent enhancement of the photocurrent.[40, 43] R_{hf} is plotted in linear scale in Figure S15. This analysis indicates that the enhancement of photovoltaic properties of aged samples is due to a reduction of the charge transfer resistance at the ZnO interface.

One of the most interesting features of the prepared cells using spray-pyrolyzed solar cells is the low hysteresis observed, see Figure S9. This low hysteresis can be attributed to the reduced low frequency capacitance, C_{lf}, observed when spray-pyrolyzed ZnO substrates are used, see Figure 6e. PSC cells using TiO_2 as electron selective contact exhibit a huge C_{lf} under illumination.[47] This capacitance is associated with an accumulation capacitance,[41, 48] and it is significantly reduced in inverted cells with no TiO_2 contact that show no hysteresis.[49] In the case of ZnO substrates, the observed values for low frequency accumulation capacitance, see Figure 6e, are significantly lower than the observed for TiO_2 substrates,[47] as the observed ones for inverted cell,[49] in good agreement with the low hysteresis obtained in this samples, see Figure S9.

4. CONCLUSIONS

In summary, here we report the preparation of ZnO thin film by spray pyrolysis with good qualities as homogeneous, full substrate coverage and high transmittance in visible range for ESC applications. Our ZnO based PSCs not only showed a good stability but also an improvement in performance after fabrication. Concretely, the conversion efficiency increased quickly (36%) after 7 days of preparation, then slightly increased after more than 1 month of preparation, with samples stored under dark at room temperature and at a humidity of around 35%. The improvement in performance is related with morphological evolution caused as the coalescence of smaller crystallites in $MAPbI_3$ films into bigger ones, resulting the enhancement in the grain size and an increase of (110) preferential orientation. We show ZnO preparation method influences this long term evolution of perovskite layer. Impedance characterization has indicated that these morphological changes of aged samples improve the charge carrier extraction at ZnO contact, enhancing

significantly photocurrent and consequently photovoltage and fill factor. ZnO substrates also present low accumulation capacitance, observed at low frequencies, and consequently presenting low hysteresis. Since the relationship between the selective contacts and the hysteresis is well known, the influence of substrate on other important properties of perovskite materials, but less studied, as morphology evolution has not been pointed out. This work highlights the effect of substrate, and concretely of selective contact on the improvement properties of halide perovskite and could contribute to produce devices with long term stability.

ASSOCIATED CONTENT

Supporting Information available free of charge on the ACS Publications website at DOI:

SEM and AFM top views; Absorbance spectra of ZnO layer at different conditions; XRD for as deposited and aged samples; Hysteresis index, IPCE and J-V curves, summary of the solar cell parameters of the prepared solar cells; LED performance; J-V curve recovering; series and high frequency resistances

ACKNOWLEDGMENTS

This work was partially supported by by the University Jaume I (project SOLENPE UJI-B2016-05) and the European Research Council (ERC) via Consolidator Grant (724424 - No-LIMIT). We acknowledge SCIC from UJI for help with XRD and SEM characterization. We thank Ehsan Hassanabadi for the measurements of substrate transmittance.

References

(1) Yang, W. S.; Park, B.-W.; Jung, E. H.; Jeon, N. J.; Kim, Y. C.; Lee, D. U.; Shin, S. S.; Seo, J.; Kim, E. K.; Noh, J. H.; Seok, S. I. Iodide management in formamidinium-lead-halide–based perovskite layers for efficient solar cells. *Science* **2017**, 356, 1376-1379.

(2) Grätzel, M. The light and shade of perovskite solar cells. *Nat. Mater.* **2014**, 13, 838.

(3) Zhang, P.; Wu, J.; Zhang, T.; Wang, Y.; Liu, D.; Chen, H.; Ji, L.; Liu, C.; Ahmad, W.; Chen, Z. D.; Li, S. Perovskite Solar Cells with ZnO Electron-Transporting Materials. *Adv. Mater.* **2017**, 1703737.

(4) Green, M. A.; Ho-Baillie, A.; Snaith, H. J. The emergence of perovskite solar cells. *Nat. Photon.* **2014**, 8, 506-514.

(5) Chueh, C.-C.; Li, C.-Z.; Jen, A. K. Y. Recent progress and perspective in solution-processed Interfacial materials for efficient and stable polymer and organometal perovskite solar cells. *Energy Environ. Sci.* **2015**, 8, 1160-1189.
(6) Fakharuddin, A.; Schmidt-Mende, L.; Garcia-Belmonte, G.; Jose, R.; Mora-Sero, I. Interfaces in Perovskite Solar Cells. *Adv. Energy Mater.* **2017**, 7, 1700623.
(7) Zhang, C.; Luo, Q.; Wu, H.; Li, H.; Lai, J.; Ji, G.; Yan, L.; Wang, X.; Zhang, D.; Lin, J.; Chen, L.; Yang, J.; Ma, C. Roll-to-roll micro-gravure printed large-area zinc oxide thin film as the electron transport layer for solution-processed polymer solar cells. *Org. Electron.* **2017**, 45, 190-197.
(8) Liu, D.; Kelly, T. L. Perovskite solar cells with a planar heterojunction structure prepared using room-temperature solution processing techniques. *Nat. Photon.* **2014**, 8, 133-138.
(9) Liu, H.; Huang, Z.; Wei, S.; Zheng, L.; Xiao, L.; Gong, Q. Nano-structured electron transporting materials for perovskite solar cells. *Nanoscale* **2016**, 8, 6209-6221.
(10) Zhang, Q.; Dandeneau, C. S.; Zhou, X.; Cao, G. ZnO Nanostructures for Dye-Sensitized Solar Cells. *Adv. Mater.* **2009**, 21, 4087-4108.
(11) Dong, X.; Hu, H.; Lin, B.; Ding, J.; Yuan, N. The effect of ALD-Zno layers on the formation of CH3NH3PbI3 with different perovskite precursors and sintering temperatures. *Chem. Commun.* **2014**, 50, 14405-14408.
(12) Vayssieres, L. Growth of Arrayed Nanorods and Nanowires of ZnO from Aqueous Solutions. *Adv. Mater.* **2003**, 15, 464-466.
(13) Mensah, S. L.; Kayastha, V. K.; Ivanov, I. N.; Geohegan, D. B.; Yap, Y. K. Formation of single crystalline ZnO nanotubes without catalysts and templates. *Appl. Phys. Lett.* **2007**, 90, 113108.
(14) Ronning, C.; Gao, P. X.; Ding, Y.; Wang, Z. L.; Schwen, D. Manganese-doped ZnO nanobelts for spintronics. *Appl. Phys. Lett.* **2004**, 84, 783-785.
(15) Ding, Y.; Kong, X. Y.; Wang, Z. L. Doping and planar defects in the formation of single-crystal ZnO nanorings. *Phys. Rev. B* **2004**, 70, 235408.
(16) Wang, Y.; Li, X.; Wang, N.; Quan, X.; Chen, Y. Controllable synthesis of ZnO nanoflowers and their morphology-dependent photocatalytic activities. *Sep. Purif. Technol.* **2008**, 62, 727-732.
(17) Gao, P. X.; Ding, Y.; Wang, Z. L. Crystallographic Orientation-Aligned ZnO Nanorods Grown by a Tin Catalyst. *Nano Lett.* **2003**, 3, 1315-1320.
(18) Heo, J. H.; Lee, M. H.; Han, H. J.; Patil, B. R.; Yu, J. S.; Im, S. H. Highly efficient low temperature solution processable planar type CH3NH3PbI3 perovskite flexible solar cells. *J. Mater. Chem. A* **2016**, 4, 1572-1578.
(19) An, Q.; Fassl, P.; Hofstetter, Y. J.; Becker-Koch, D.; Bausch, A.; Hopkinson, P. E.; Vaynzof, Y. High performance planar perovskite solar cells by ZnO electron transport layer engineering. *Nano Energy* **2017**, 39, 400-408.
(20) Lin, L.; Jiang, L.; Qiu, Y.; Yu, Y. Modeling and analysis of HTM-free perovskite solar cells based on ZnO electron transport layer. *Superlattices Microstruct.* **2017**, 104, 167-177.
(21) Azmi, R.; Hadmojo, W. T.; Sinaga, S.; Lee, C.-L.; Yoon, S. C.; Jung, I. H.; Jang, S.-Y. High-Efficiency Low-Temperature ZnO Based Perovskite Solar Cells Based on Highly Polar, Nonwetting Self-Assembled Molecular Layers. *Adv. Energy Mater.*, **2018**, 8, 1701683.

(22) Zhang, J.; Juarez-Perez, E. J.; Mora-Sero, I.; Viana, B.; Pauporte, T. Fast and low temperature growth of electron transport layers for efficient perovskite solar cells. *J. Mater. Chem. A* **2015**, 3, 4909-4915.
(23) Jiaxing, S.; Ji, B.; Enqiang, Z.; Xiao-Feng, W.; Wenjing, T.; Tsutomu, M. Efficient and Environmentally Stable Perovskite Solar Cells Based on ZnO Electron Collection Layer. *Chem. Lett.* **2015**, 44, 610-612.
(24) Hu, Q.; Liu, Y.; Li, Y.; Ying, L.; Liu, T.; Huang, F.; Wang, S.; Huang, W.; Zhu, R.; Gong, Q. Efficient and low-temperature processed perovskite solar cells based on a cross-linkable hybrid interlayer. *J. Mater. Chem. A* **2015**, 3, 18483-18491.
(25) Song, J.; Liu, L.; Wang, X.-F.; Chen, G.; Tian, W.; Miyasaka, T. Highly efficient and stable low-temperature processed ZnO solar cells with triple cation perovskite absorber. *J. Mater. Chem. A* **2017**, 5, 13439-13447.
(26) Vimalkumar, T. V. Highly conductive and transparent ZnO thin film using Chemical Spray Pyrolysis technique: Effect of doping and deposition parameters. Cochin University of Science and Technology, 2011.
(27) Prasada Rao, T.; Santhosh Kumar, M. C.; Ganesan, V. Effect of annealing on the structural, optical and electrical properties of ZnO thin films by spray pyrolysis. *Indian J. Phys.* **2011**, 85, 1381.
(28) Tseng, Z.-L.; Chiang, C.-H.; Wu, C.-G. Surface Engineering of ZnO Thin Film for High Efficiency Planar Perovskite Solar Cells. *Sci. Rep.* **2015**, 5, 13211.
(29) Roose, B.; Ummadisingu, A.; Correa-Baena, J.-P.; Saliba, M.; Hagfeldt, A.; Graetzel, M.; Steiner, U.; Abate, A. Spontaneous crystal coalescence enables highly efficient perovskite solar cells. *Nano Energy* **2017**, 39, 24-29.
(30) Yen-Chen, S.; Yu-Bing, L.; Chia-Shuo, L.; Hsiao-Chi, H.; Leeyih, W.; Chih-I, W.; King-Fu, L. Amino-Acid-Induced Preferential Orientation of Perovskite Crystals for Enhancing Interfacial Charge Transfer and Photovoltaic Performance. *Small* **2017**, 13, 1604305.
(31) Climent-Pascual, E.; Hames, B. C.; Moreno-Ramirez, J. S.; Alvarez, A. L.; Juarez-Perez, E. J.; Mas-Marza, E.; Mora-Sero, I.; de Andres, A.; Coya, C. Influence of the substrate on the bulk properties of hybrid lead halide perovskite films. *J. Mater. Chem. A* **2016**, 4, 18153-18163.
(32) Peng, Y.; Cheng, Y.; Wang, C.; Zhang, C.; Xia, H.; Huang, K.; Tong, S.; Hao, X.; Yang, J. Fully doctor-bladed planar heterojunction perovskite solar cells under ambient condition. *Org. Electron.* **2018**, 58, 153-158.
(33) Chunhua, W.; Chujun, Z.; Shitan, W.; Gang, L.; Huayan, X.; Sichao, T.; Jun, H.; Dongmei, N.; Conghua, Z.; Kongxian, D.; Yongli, G.; Junliang, Y. Low-Temperature Processed, Efficient, and Highly Reproducible Cesium-Doped Triple Cation Perovskite Planar Heterojunction Solar Cells. *Solar RRL* **2018**, 2, 1700209.
(34) Huang, K.; Wang, C.; Zhang, C.; Tong, S.; Li, H.; Liu, B.; Gao, Y.; Dong, Y.; Gao, Y.; Peng, Y.; Yang, J. Efficient and stable planar heterojunction perovskite solar cells fabricated under ambient conditions with high humidity. *Org. Electron.* **2018**, 55, 140-145.
(35) Aristidou, N.; Eames, C.; Sanchez-Molina, I.; Bu, X.; Kosco, J.; Islam, M. S.; Haque, S. A. Fast oxygen diffusion and iodide defects mediate oxygen-induced degradation of perovskite solar cells. *Nat. Commun.* **2017**, 8, 15218.
(36) Bryant, D.; Aristidou, N.; Pont, S.; Sanchez-Molina, I.; Chotchunangatchaval, T.; Wheeler, S.; Durrant, J. R.; Haque, S. A. Light and oxygen induced degradation

limits the operational stability of methylammonium lead triiodide perovskite solar cells. *Energy Environ. Sci.* **2016**, 9, 1655-1660.
(37) Yang, J.; Siempelkamp, B. D.; Mosconi, E.; De Angelis, F.; Kelly, T. L. Origin of the Thermal Instability in CH3NH3PbI3 Thin Films Deposited on ZnO. *Chem. Mater.* **2015**, 27, 4229-4236.
(38) Aristidou, N.; Sanchez-Molina, I.; Chotchuangchutchaval, T.; Brown, M.; Martinez, L.; Rath, T.; Haque, S. A. The Role of Oxygen in the Degradation of Methylammonium Lead Trihalide Perovskite Photoactive Layers. *Angew. Chem., Int. Ed.* **2015**, 54, 8208-8212.
(39) Koocher, N. Z.; Saldana-Greco, D.; Wang, F.; Liu, S.; Rappe, A. M. Polarization Dependence of Water Adsorption to CH3NH3PbI3 (001) Surfaces. *J. Phys. Chem. Lett.* **2015**, 6, 4371-4378.
(40) Guerrero, A.; Garcia-Belmonte, G.; Mora-Sero, I.; Bisquert, J.; Kang, Y. S.; Jacobsson, T. J.; Correa-Baena, J.-P.; Hagfeldt, A. Properties of Contact and Bulk Impedances in Hybrid Lead Halide Perovskite Solar Cells Including Inductive Loop Elements. *J. Chem. Phys. C* **2016**, 120, 8023-8032.
(41) Zarazua, I.; Han, G.; Boix, P. P.; Mhaisalkar, S.; Fabregat-Santiago, F.; Mora-Seró, I.; Bisquert, J.; Garcia-Belmonte, G. Surface Recombination and Collection Efficiency in Perovskite Solar Cells from Impedance Analysis. *J. Chem. Phys. Lett.* **2016**, 7, 5105-5113.
(42) Zarazúa, I.; Sidhik, S.; Lopéz-Luke, T.; Esparza, D.; De la Rosa, E.; Reyes-Gomez, J.; Mora-Seró, I.; Garcia-Belmonte, G. Operating Mechanisms of Mesoscopic Perovskite Solar Cells through Impedance Spectroscopy and J–V Modeling. *J. Chem. Phys. Lett.* **2017**, 8, 6073-6079.
(43) Juarez-Perez, E. J.; Wuβler, M.; Fabregat-Santiago, F.; Lakus-Wollny, K.; Mankel, E.; Mayer, T.; Jaegermann, W.; Mora-Sero, I. Role of the Selective Contacts in the Performance of Lead Halide Perovskite Solar Cells. *J. Chem. Phys. Lett.* **2014**, 5, 680-685.
(44) Dualeh, A.; Moehl, T.; Tétreault, N.; Teuscher, J.; Gao, P.; Nazeeruddin, M. K.; Grätzel, M. Impedance Spectroscopic Analysis of Lead Iodide Perovskite-Sensitized Solid-State Solar Cells. *ACS Nano* **2014**, 8, 362-373.
(45) Pockett, A.; Eperon, G. E.; Peltola, T.; Snaith, H. J.; Walker, A.; Peter, L. M.; Cameron, P. J. Characterization of Planar Lead Halide Perovskite Solar Cells by Impedance Spectroscopy, Open-Circuit Photovoltage Decay, and Intensity-Modulated Photovoltage/Photocurrent Spectroscopy. *J. Chem. Phys. C* **2015**, 119, 3456-3465.
(46) Guillén, E.; Ramos, F. J.; Anta, J. A.; Ahmad, S. Elucidating Transport-Recombination Mechanisms in Perovskite Solar Cells by Small-Perturbation Techniques. *J. Chem. Phys. C* **2014**, 118, 22913-22922.
(47) Juarez-Perez, E. J.; Sanchez, R. S.; Badia, L.; Garcia-Belmonte, G.; Kang, Y. S.; Mora-Sero, I.; Bisquert, J. Photoinduced Giant Dielectric Constant in Lead Halide Perovskite Solar Cells. *J. Chem. Phys. Lett.* **2014**, 5, 2390-2394.
(48) Zarazua, I.; Bisquert, J.; Garcia-Belmonte, G. Light-Induced Space-Charge Accumulation Zone as Photovoltaic Mechanism in Perovskite Solar Cells. *J. Chem. Phys. Lett.* **2016**, 7, 525-528.
(49) Kim, H.-S.; Jang, I.-H.; Ahn, N.; Choi, M.; Guerrero, A.; Bisquert, J.; Park, N.-G. Control of I–V Hysteresis in $CH_3NH_3PbI_3$ Perovskite Solar Cell. *J. Chem. Phys. Lett.* **2015**, 6, 4633-4639.

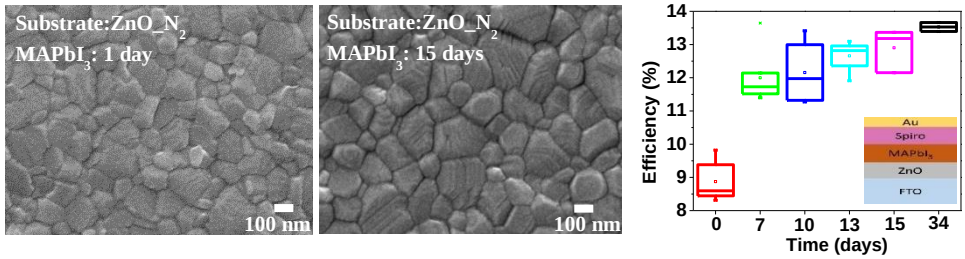
Substrate:ZnO_N2
MAPbI3: 1 day
100 nm
Substrate:ZnO_N2
MAPbI3: 15 days
100 nm
Efficiency (%)
Time (days)
Au
Spiro
MAPbI3
ZnO
FTO

TOC Figure